Engineering Journal issn: 0125-8281

Article

Enhancement of Photoluminescence Collection from Diamond-Based Quantum Emitter with Diamond Photonic Nanopillar

Preeti Ovartchaiyapong

Department of Electrical and Computer Engineering, Thammasat University, Pathum Thani, Thailand
*E-mail: opreeti@engr.tu.ac.th (Corresponding author)

Abstract. This work aimed to examine the effects of photonic diamond nanopillar toward enhancing the collection efficiency of photoluminescence signal from quantum emitters in diamond. In this work, the finite element methods were used as a platform to characterize the emission pattern and the collection efficiency. The collection efficiency value was then characterize based on various variables, including pillar diameters, dipole orientation, emission wavelength, and emitter placement inside the photonic structure. From the simulations, the collection efficiency from an optimized nanopillar structure can be improved up to three times the bulk value, particularly in pillar diameters ranging from 70-100nm. Furthermore, the multivariable dependency studies provide valuable insight into the design and engineering tolerance of future practical quantum-based devices.

Keywords: Photonic structure, optical waveguide, nitrogen-vacancy center, quantum technology, nanotechnology.

ENGINEERING JOURNAL Volume 26 Issue 8
Received 12 April 2022
Accepted 22 August 2022
Published 31 August 2022
Online at https://engj.org/
DOI:10.4186/ej.2022.26.8.41

DOI:10.4186/ej.2022.26.8.41

1. Introduction and Background

1.1. Quantum Technology

For the last half-century, technology in Electrical and Computer Engineering based on transistors and integrated circuits have been the cornerstone of our modern world [1, 2]. These technologies pave the ways for advancements in high-performance computation and powerful portable devices. There has been significant progress in improving the existing manufacturing platform, such as making the transistor smaller resulting in a higher number of computation units. The famously observed trend known as Moore's Law predicted doubling the number of transistors on integrated circuit chips every two years [3]. However, to preserve the computation speed, the rising number of transistors necessitate the size of the transistor to go down, recently as small as 5 nm [4]. To continue this trend, the innovators have to face the imminent nanoscale dynamics among the densely packed transistors such as tunneling effects based on quantum mechanics.

In attempts to overcome the existing restrictions, a novel field has been proposed based on quantum mechanics itself, broadly referred to as quantum technology. In this field, quantum properties of two-state systems are known as quantum bits or Qubits. In special situations, quantum bits can be used to form quantum computers, which achieves exceptional computational power, such as breaking down large prime numbers factorization in the widely used RSA cryptography scheme [5]. On the other hand, quantum cryptography can accomplish unbreakable communication platforms based on quantum key distribution protocols. Lastly, quantum systems can be utilized as sensors with sensitivities beyond those of conventional integrated circuit sensors by dynamically decoupling themselves from the classically unavoidable thermal noise.

1.2. Quantum Bit Systems

There are many fascinating qubits candidates such as, localized quantum dots [6], superconducting circuits [7] and optical transitions of trapped atoms [8], trapped ions [9] and electronics defects in solid-state defects [10]. These quantum systems have some basic requirements to be useful, such as abilities to perform initialization, manipulation, readout, and coherence (retaining information) [11]. Since quantum systems are sensitive to the environment, they usually lose their coherence under ambient conditions. To remain isolated from the external excitation, most qubits are required to be in extremely low temperatures approaching zero kelvin, where sophisticated cooling or isolation equipment is needed. This requirement is one of the obstacles to developing a practical quantum-based platform.

Recently, solid-state quantum systems have been found to exhibit quantum control at ambient conditions, particularly the nitrogen-vacancy (NV) center in diamonds. The diamond-based quantum system has been found to have a long coherence time up to a few milliseconds at room temperature, which can also be further extended to second-scale coherence at low temperature [12, 13]. Additionally, the nitrogen-vacancy center system has been demonstrated to have various fields sensitivity, making the system an excellent candidate for quantum-based sensing applications.

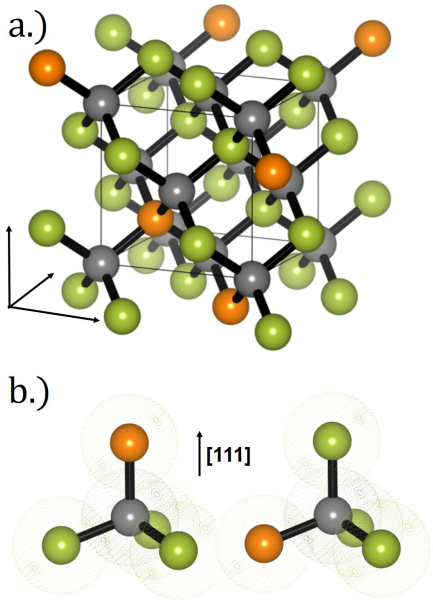

Fig. 1. (a.) A diamond unit cell consisting of carbon atoms (green), with nitrogen-vacancy centers at various locations. The grey atoms represent vacancy sites, while the orange atoms represent nitrogen sites. (b.) Individual nitrogen vacancies in a [111] diamond, representing the on-axis oriented NV center (left) and the off-axis oriented NV centers (right)

1.3. The Nitrogen-Vacancy Center: Background

The nitrogen-vacancy center in diamond is one of the many defects in the diamond's lattice. It replaces two adjacent carbon atoms with a nitrogen atom and an empty space, i.e. a vacancy, as shown in Fig. 1. Because of its nanoscale size, nitrogen-vacancy centers have been proposed to be used in high-resolution magnetic field mapping, with sensitivity below thermal noise fluctuation. Additionally, the defect can occupy four orientations in the diamond's lattice, which can be used to map the full components of the Electromagnetic field vector [14, 15]. The defect introduces a disruption in the diamond's carbon-carbon covalent bonds, creating electronic systems. Particularly, the nitrogen-vacancy center can capture one extra electron to become NV^{-}, constituting a spin-1. Because of the diamond's large 5.5 eV bandgap, the nitrogen-vacancy center's electron system is protected from external excitation. Additionally, diamond's high Debye temperature shelves the

defect from phonon excitation.

A simplified version of the nitrogen-vacancy center's electronic structure is shown in Fig. 2, with the zero-phonon-line transition of approximately 637 nm between the ground state and the excited state. In this two-level system, the electron can be excited resonantly using a 637 nm light source or non-resonantly into the phonon sideband with a 532 nm wavelength light source. Similarly, when an electron decays back to the ground state, it can either emit a photon with the zero-phonon-line transition or phonon sideband transition (longer wavelength photon and lattice vibrations). The photons emitted from the zero-phonon-line transitions can be used in quantum communication applications in a long-range entanglement [16, 17] and teleportation [18], which are the basis of quantum computing and quantum communication. Within the optical transition, nitrogen-vacancy center's electron spin hyperfine structures can also be used as room-temperature quantum memory [19] and quantum-based electromagnetic field sensors [20, 21]. The states of the spin qubit along with the encoded information can also be measured by reading out the emitted photon. Since both qubit systems realized in the nitrogen-vacancy center rely on the detection of the emitted photon, it is crucial to detect the photon as efficiently as possible to achieve the qubit's usability.

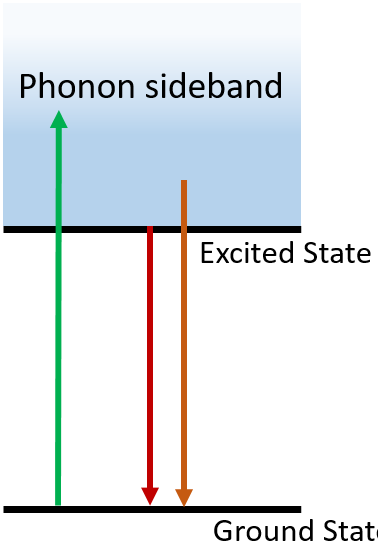

Fig. 2. A simplified diagram of the nitrogen-vacancy center electronic structure. The system is excited with a non-resonant green laser (green arrow) into the phonon sideband. The emission can be from the zero-phonon-line at approximately 637 nm (red arrow) or from a longer wavelength phonon sideband emission (orange arrow).

1.4. The Limitations

There are several problems preventing the efficient detection of the emitted photons. With fundamental characteristics, the nitrogen-vacancy center behaves like a dipole point source, which emits light in all directions. The confocal microscopy technique is often used to image the emitter. In a confocal microscopy setup, a microscope objective is used to collect the emitted photoluminescence signal. The acceptance angle of the microscope objective is limited by the numerical aperture (N.A.). In the best case, a 0.95 numerical aperture in-air microscope objective can only gather around 142 degrees out of the full 360 degrees. Furthermore, the diamond's high index of refraction prevents another portion of the photon signals from leaving the diamond-air interface through total internal reflection. This means all the photoluminescence signals exiting the diamond at an angle larger than the critical angle will be trapped inside the crystal.

In combination with other optical losses in an ordinary confocal setup, only 4-5 percent of the overall signal emission is collected [22]. This requires nitrogen-vacancy readout to be repeated and averaged over many times to obtain acceptable measurement fidelity.

1.5. Challenges: Photon Signal Collection Enhancement

To reduce the measurement averaging time, this work explores diamond waveguide structures, which can direct more photon signal toward the collection optics. There are a number of approaches that can improve the signal collection efficiency, including diamond solid immersion lenses [23], photonic diamond structures [24], and even nanodiamond particles [25]. These approaches have different degrees of enhancement and fabrication difficulty. However, diamond solid immersion lens and nanodiamond are hard to precisely control and scale into a bigger network of qubits. On the other hand, a photonic diamond structure can be mass fabricated and has been shown preliminarily to achieve some degree of photon collection enhancement [26, 27].

This work particularly explores diamond nanopillar structures due to their relatively simpler and scalable fabrication process. Nevertheless, emission enhancement of diamond nanopillar is still missing some pieces toward the complete picture both experimentally and theoretically. Additionally, past theoretical works utilized the Finite-different time-domain (FDTD) simulations. The FDTD simulation solves time-dependent Maxwell's equation in three-dimensional space, which can take a long time for the solution to converge. The computation resource needed for the FDTD simulations discourages researchers from exploring many interesting theoretical facets of nanopillar structure, limiting past works to a few simple cases with only zero-phonon line emission [26]. To build our understanding toward practical designs, there are still quite a few variables to explore in real-world applications, such as wavelength-based enhancement, nitrogen-vacancy center orientation, and the location of the nitrogen-vacancy center

in the nanopillar.

To overcome the computational resource and location of the FDTD method, this work explores a different simulation platform in the finite element method (FEM), which has been one of the main workhorses in engineering simulations [28]. In the FEM, the simulation only solves differential equations in three-dimensional space without the time-domain considerations like in the FDTD platform. Hence, some problems without the need for time-domain solutions can be solved faster with the FEM simulation. This allows the FEM simulation to explore more variables and testing scenarios in a reasonable amount of time.

Utilizing the FEM simulation, this work will explore and optimize the nanopillar designs by first considering the pillar dimensions, along with the broad spectrum emission from the nitrogen-vacancy center. Finally, the nitrogen-vacancy center position in the nanopillar will be considered to find the optimum location for various quantum-based applications.

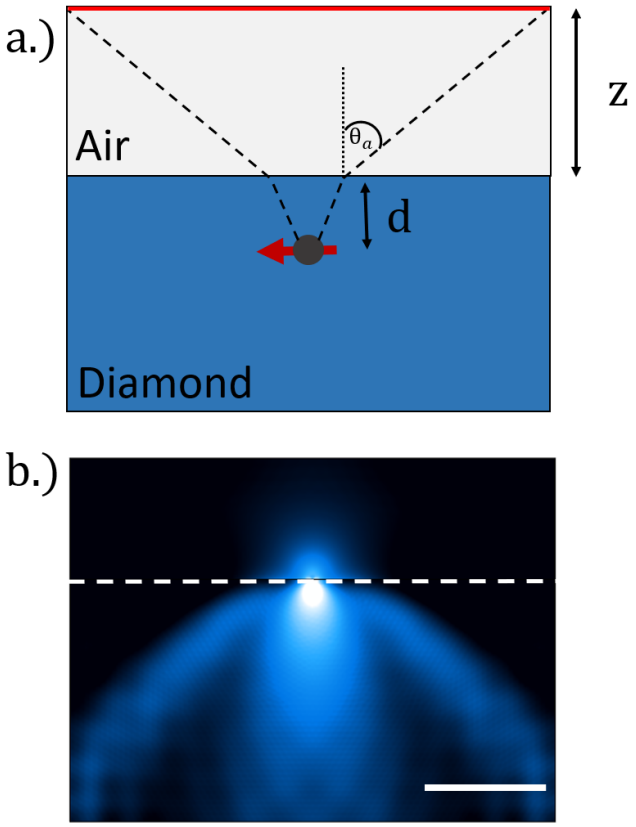

Fig. 3. (a) A diagram of the simulation domain, where the height of the air domain h is a function of the acceptance angle θ_a set by the numerical aperture value of the microscope objective. (b) An example plot of an [111] oriented nitrogen-vacancy center emission, where the dashed line is the diamond-air interface. The length of the scale bar is 650 nm.

2. Theory and Modeling

2.1. Photoluminescence emission theory

Like any electromagnetic wave radiation, the underlying principle of the nitrogen-vacancy center dipole emission is govern by Maxwell's equation in different mediums from diamond to air.

$$\nabla \times \vec{E} = -\frac{\partial \vec{B}}{\partial t} \tag{1}$$

$$\nabla \times \vec{B} = -\frac{1}{v^2}\frac{\partial \vec{E}}{\partial t} \tag{2}$$

, where $\vec{E}$ and $\vec{B}$ are electric field wave vectors and magnetic field wave vectors respectively. v is the speed of an electromagnetic wave in the medium which is governed by the electromagnetic properties of materials

$$v = \frac{1}{\sqrt{\epsilon_0 \epsilon_r \mu_0 \mu_r}} \tag{3}$$

, where ϵ_0 is the permittivity of free space, ϵ_r is the relative permittivity or known as the dielectric constant of the material, μ_0 is the vacuum permeability and μ_r is the relative permeability. For electromagnetic waves traveling through a vacuum where $\mu_r = 1$ and $\epsilon_r = 1$, the speed of electromagnetic wave reduces to

$$v_{\text{vac}} = \frac{1}{\sqrt{\epsilon_0 \mu_0}} \equiv c \tag{4}$$

, where c is universally known as the speed of light traveling through a vacuum. This also means the speed of electromagnetic waves in a material can be determined by the material's relative permeability and relative permittivity,

$$v = \frac{c}{\sqrt{\epsilon_r \mu_r}} \equiv \frac{c}{n} \tag{5}$$

, where n is defined as the 'refractive index' of the material. To maintain the same electromagnetic wave frequency when traveling between different mediums, the wavelength of the radiation will have to change. To retain the wave continuity, the electromagnetic waves will change their travel path when passing through an interface with two different materials. This deviation in electromagnetic wave path can be described with a well-known equation called Snells' Law.

$$n_1 \sin\theta_1 = n_2 \sin\theta_2 \tag{6}$$

, where θ_1 is the incident angle of the wave entering the interface from the medium with n_1 refractive index and θ_2 is the refractive wave angle. Both angles are measured with respect to the interface's normal vector.

The nitrogen-vacancy center will be treated as a dipole point source that emits electromagnetic radiation. Because of the diamond's large index of refraction, the refractive angle will be considerably larger than the incident angle. Hence, emissions at a moderately large incident angle will require the value of $\sin\theta_2$ to be larger than one, making it mathematically impossible for the radiation to refract out

of the diamond. This phenomenon is commonly known as total internal reflection. As a result, only a portion of the light will be able to exit the diamond-air interface. Furthermore, the collection microscope objective is only accepting light a portion within its acceptance angle (θ_{a}) defined by the numerical aperture (N.A.) specification,

$$\text{N.A.} = n \sin \theta_{\mathrm{a}} \tag{7}$$

, where n is the index of refraction in the environment surrounding the objective's glass. In the case of an air objective, n is approximately one. The highest numerical aperture air microscope objective available commercially only has 0.95, which corresponds to approximately 71 degrees acceptance cone. These factors described here emphasize the challenges in capturing the optical signal from the nitrogen-vacancy center's emission.

2.2. Finite element modeling setup

Unlike FDTD simulations, the simulation setup for the finite element modeling is not straightforward in handling polar coordinates calculation because of its Cartesian-based differential equation solver. The acceptance cone angle has to be constructed manually by defining the width and height of the air domain in the air-diamond interface. A [111] diamond substrate is considered in this work due to its prospect in quantum sensing and quantum computing. Because of the rotational symmetry of the dipole orientation in a [111] diamond substrate, the emission pattern is the same regardless of rotation around the symmetry axis. Hence, the simulation can be performed and normalized in two dimensions [26]. The first goal was to set up a platform for simulating the collection efficiency of emission from a nitrogen-vacancy center in the bulk diamond substrate at different numerical aperture values. The nitrogen-vacancy center was assumed to be at the depth d inside a bulk diamond substrate with a fixed domain width w, as shown in Fig. 3(a). The dipole orientation is perpendicular to the bond angle of the nitrogen-vacancy center, which can be separated into x and y dipole components in the simulation. Additionally, the scattering boundary condition was used in the non-interface boundary to eliminate any simulation artifacts from boundary reflections. With a fixed simulation domain width w, the height of the air domain h can then be varied to dictate the acceptance cone angle, i.e. the lower the domain height the larger the acceptance cone angle. Because of the difference in electromagnetic properties of diamond and air, the acceptance cone angle in air will be different from the acceptable emission angle from the nitrogen-vacancy center emission in the diamond. For a deeply placed nitrogen-vacancy center, more calculation was needed to calculate the relationship between the domain height h and the numerical aperture (**NA**). Using simple trigonometry identities and Snell's Law, the domain height as a function of the microscope objectives numerical aperture was calculated to be

$$h = \left(\frac{w}{2} - d \left(\frac{n_d^2}{\mathbf{NA}^2} - 1 \right)^{-\frac{1}{2}} \right) \left(\mathbf{NA}^{-2} - 1 \right)^{\frac{1}{2}} \tag{8}$$

, where $n_d = 2.432$ is the diamond's index of refraction. In the situations for shallow dipoles $d \ll w$, the air domain height h expression reduces to

$$h = \frac{w}{2} \left(\mathbf{NA}^{-2} - 1 \right)^{\frac{1}{2}}. \tag{9}$$

Although a large w value can be selected to simplify the expression, the large domain size will require more simulation time. As a result, the electromagnetic wave power flowing through each boundary was calculated by performing a line integral of the Poynting vector component normal to the boundary of interest. The collection efficiency (η) can then be calculated by realizing the ratio between the power flow through the top air domain (red line in Fig. 3a) and the power flow through all outside domain boundaries,

$$\eta = \frac{\int_{\text{top}} \vec{S}(x,y) \cdot \hat{y} dl}{\int_{\text{all}} \vec{S}(x,y) \cdot \hat{n} dl} \tag{10}$$

, where $\vec{S}(x,y)$ is the emitted wave's Poynting vector, and $\vec{n}$ is the normal vector to each boundary.

An example plot of the simulation is shown in Fig. 3. To verify the initial results, the calculated collection efficiency values at various numerical aperture were compared to existing published experimental results and FDTD simulations. The results obtained with the Finite Element simulation platforms agree well with the previously published experimental values [22].

2.2.1. Photonic Pillar Modelling

With the demonstrated photon collection simulation platform, any arbitrary structures can be explored to study the signal detection enhancement. In this work, simple photonic cylindrical pillars were explored due to their practical and scalable fabrication process. The photonic pillars were simulated as a cylindrical diamond waveguide, which will direct the emission toward the microscope objective. Similar to the bulk diamond simulation, the air height measured from the top of the pillar is set by the microscope objective's numerical aperture. The photon collection efficiency can be calculated by comparing the power flowing through the top domain and all the outflow power, using Eq. 10. An example plot of the waveguide effect from the nanopillar is shown in Fig. 4b. In this model, the dimensions of the pillar, dipole location, and dipole emission wavelength can be varied, which will be discussed in the result section. Because

DOI:10.4186/ej.2022.26.8.41

of the faster simulation time, more variables can be tested in this work compared to the previous results done by FDTD simulations [26]. The collection efficiency improvements in different configurations will shed light on the possible best designs for real-world applications.

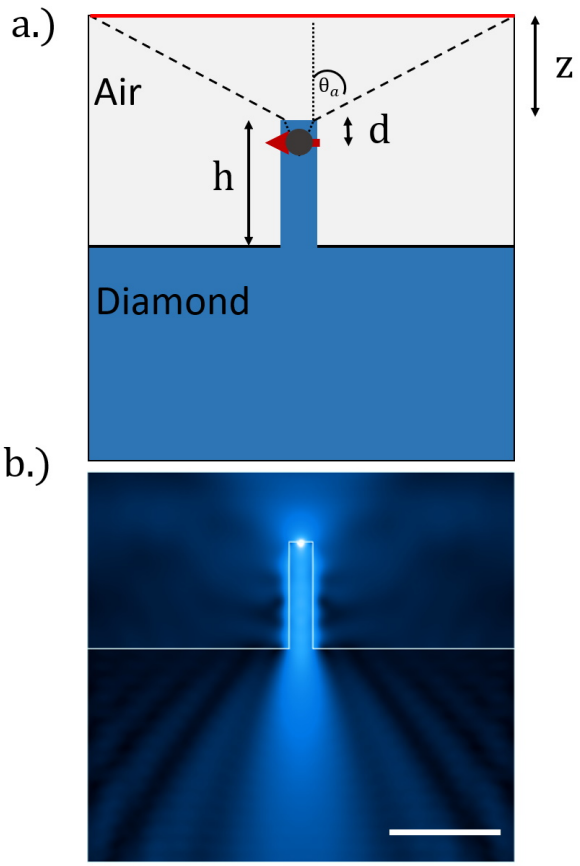

Fig. 4. (a) A diagram of the diamond pillar simulation, where the height of the air domain z is set by the acceptance angle θ_a, h is the pillar's height and w is the pillar's diameter. (b) An example plot of an [111] oriented nitrogen-vacancy center emission inside a photonic cylindrical pillar. The length of the scale bar is 1000 nm.

3. Results and Discussions

Many variables can have an influence on the collection efficiency including pillar dimensions, emission wavelength, and emitter placement inside the pillar. All variables cannot be examined at the same time because of the unknown variable convolution. Furthermore, it would be almost impossible to extract the individual contribution from each variable in an enormous set of convoluted data. Hence, the main strategy of this work is to find the optimum case for each variable and inspect how the variables are related in each section.

3.1. Pillar diameter and dipole orientation

Similar to optical fibers, the diameter of the pillar directly affects how light waves propagate inside the waveguide. Additionally, the emitter's dipole orientations have their specific radiation pattern, which responds differently to the waveguide. For this reason, it is sensible to first explore the pillar diameter and dipole orientation dependency to establish a starting point for other variables. In this study, the nitrogen-vacancy center depth was set to be 15 nm with the pillar height of 1 μm, which were parameters similar to the ones in previous work [26]. In this first section, the emission was only limited to the zero-phonon-line 637 nm wavelength. The pillar diameter was varied from 10 nm to 4000 nm to study the effect of the pillar diameter on the collection efficiency. However, the collection efficiency had reached the value of emission from the bulk diamond for pillar diameter over 1000 nm. The study was performed for both on-axis and off-axis emitters as described in Fig. 1b. The collection efficiency's dependency on the pillar diameter up to 1000 nm was illustrated in Fig. 5.

From the simulated result, the off-axis oriented nitrogen-vacancy centers can be improved to 30 percent collection efficiency. On the other hand, the on-axis oriented emitter sees a much larger improvement up to nearly 60 percent collection efficiency near 100 nm diameter, which is approximately three times the value of the bulk diamond emission of around 20 percent. Although both orientations are promising, the collection efficiency in the on-axis emitter observes much greater benefits from the photonic pillar structure. This is somewhat expected due to the emission pattern along the direction of the photonic pillar, as previously explained in other work [29, 30] Nevertheless, the on-axis type emitters have a much tighter window of approximately 20 nm for pillar diameter to achieve maximum enhancement, which could be challenging in the real-world fabrication process.

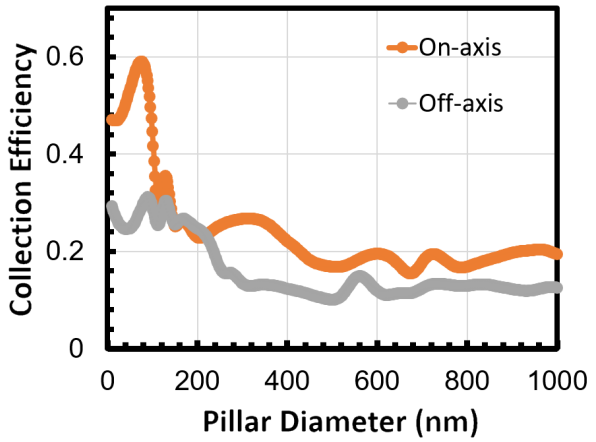

Fig. 5. A plot showing the collection efficiency for varying pillar diameter up to 1000 nm for on-axis oriented NV center (orange) and off-axis oriented NV center(gray).

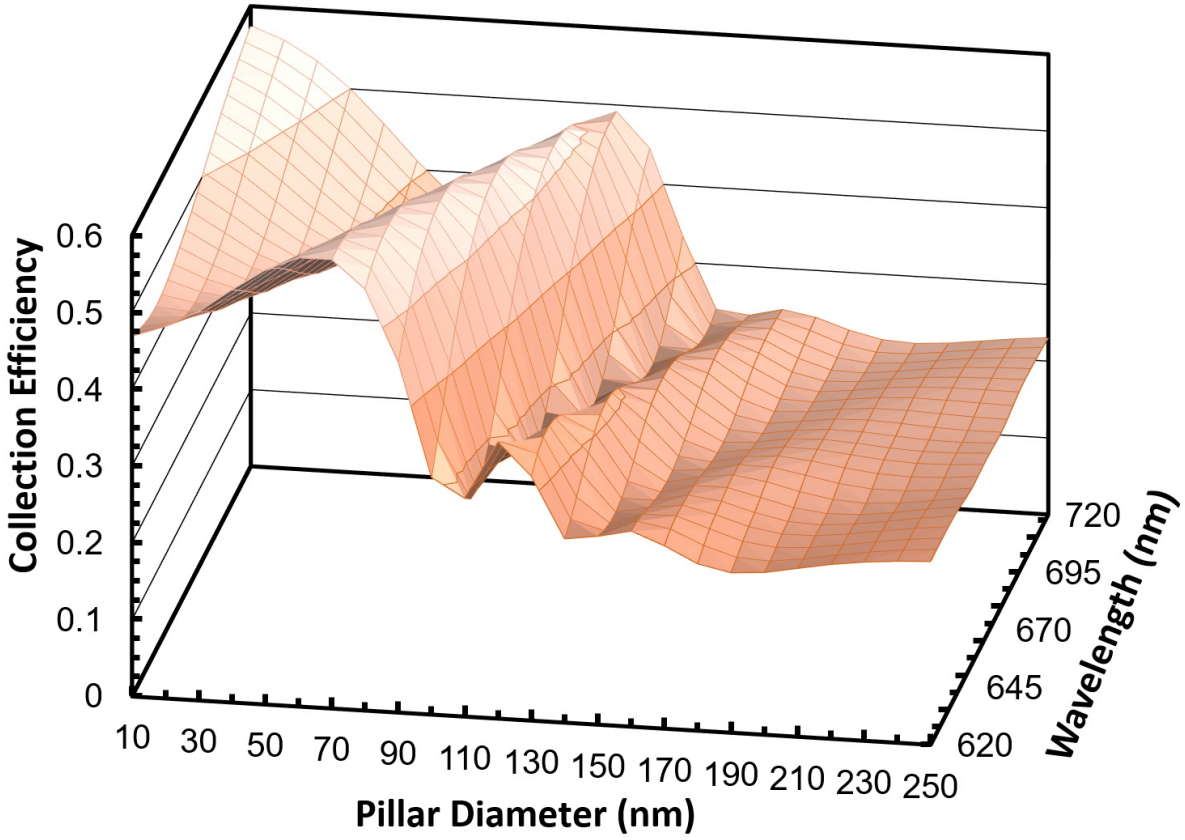

Fig. 6. A surface plot showing the collection efficiency for varying pillar diameters for the on-axis NV center for the emitted wavelengths ranging from 600 nm to 720 nm.

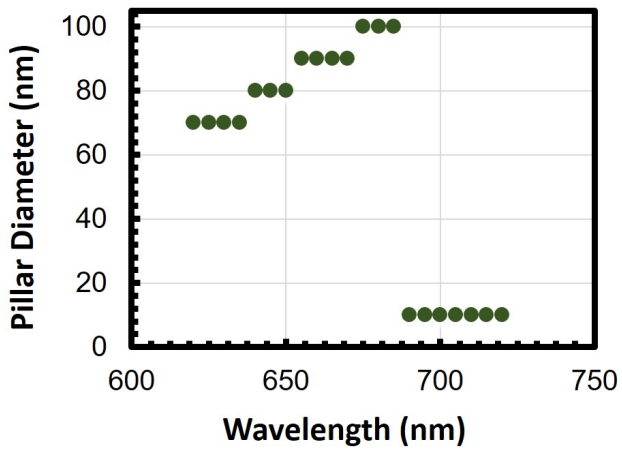

Fig. 7. A plot showing the pillar diameters with the highest collection efficiency as a function of their corresponding emission wavelength. The data suggests an optimum diameter in the range of 70-100 nm.

3.2. Emitted wavelength dependency

As mentioned earlier, the nitrogen-vacancy center not only emits photons in the zero-phonon-line but also emits from the phonon-sideband with wavelengths from 600 to 800 nm. Though lacking indistinguishable properties for entanglement applications, these photons contain information on the electron's spin quantum state. The electron spins interact with the various fields in the environment, which allows the spins to be used in sensing applications. Hence, the wavelength dependency of the signal collection enhancement can be crucial information in designing a sensor.

In this study, the collection efficiency values were explored for emission wavelengths ranging from 620 nm to 720 nm. This selection already contained the majority of the nitrogen-vacancy center's emission spectrum. The pillar diameters were only considered up to 250 nm because the collection efficiency improvements have diminished for larger diameters as observed in Fig. 5. The result is presented using a surface plot as shown in Fig. 6. Following similar trends to the zero-phonon-line emission, the data suggests that the optimum diameters slightly scale larger for

a longer emission wavelength. Interestingly, there seem to be extra maxima for a longer emission wavelength near 700 nm. However, the extra optimum requires the pillar to be around 10 nm, which is too small to be reliably fabricated using current fabrication techniques.

Finally, the information from the surface plot was extracted into a plot of pillar diameters which allow for the highest collection efficiency versus the corresponding emitted wavelength in Fig. 7. For longer emission wavelengths over 690 nm, the maximum collection efficiency is expected to be achieved in the 10 nm pillar. In more realistic applications, the optimum diameter for the majority of the emitted spectrum would be around 70 to 100 nm. This diameter range is already close to the current accuracy limit for diamond nanofabrication, which is around 10 to 20 nm. Hence, picking the precise number within 70-100 nm is not too critical as the fabricated pillars can have around 10-20 nm discrepancy.

3.3. Emitter placement in the photonic pillar

The simulated studies above have shed light on the range of photonic pillar structures, which will allow for reasonably efficient signal collection. However, this ideal study has not considered the emitter's location which cannot be placed precisely in real applications. The emitter placement is usually limited by the ion implantation process, where the lateral placement of the defect will be random. A certain amount of lateral control can be achieved by the electron beam lithography technique. However, the error might still be approximately a few tens of nanometers. The depth uncertainty is also intrinsic to the ion implantation process, ranging from a few nanometers for shallow implantation to tens of nanometers for deeper implantation. In this section, the effect of location uncertainty will be inspected for both lateral and depth placement.

3.3.1. Emitter's depth placement

The most common process of nitrogen-vacancy center creation is ion implantation. In the process, the high-energy nitrogen ions electronically interact with the diamond's lattice making the ion stop at a certain depth depending on the ion's energy. However, the random nature of the process causes some deviation from the average depth value, called straggling. This uncertainty could cause the real structure to behave differently from the initial ideal simulation. Hence, the effects of depth dependency were inspected using the presented simulation platform, as shown in Fig. 8. With the zero-phonon-line emission, the simulation was performed for both 70 nm (red) and 100 nm (orange) pillar diameter, which approximately represents the range of optimum pillar dimensions from the previous section.

The results reveal an interesting convolution between the depth placement and the pillar diameter in achieving the highest collection efficiency for a particular emission wavelength. Both structures exhibit oscillation in optimum value throughout the studied emitter's depth placement. For the 70 nm pillar diameter, the first peak was observed near the surface of the diamond. This was expected as it was the original condition of the previous pillar diameter simulation. However, the first optimum depth was observed near 80 nm inside the diamond. This means the optimum design will depend on the wavelength of interest, pillar diameter, and the emitter's depth. The maximum achievable efficiency value approximately approaches 60 percent for both cases. Although the values are all convoluted making it impossible for realizing the best structure for all applications, sufficiently robust values can be selected such as near the maxima where the gradient of the collection efficiency change is smaller. This will help manage the structure fabrication tolerance in comparison to the depth's straggle in the ion implantation process.

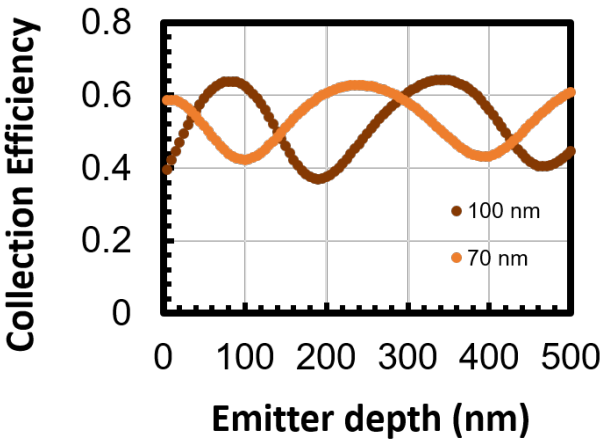

Fig. 8. A plot showing the dependency of the collection efficiency on the depth placement of the emitter. Two sets of pillar diameter 70 nm (orange) and 100 nm (red) were studied and found to have different optimum depths.

3.3.2. Lateral emitter placement

Because the structure has cylindrical symmetry around the pillar axis, the lateral placement can always be described by the radial displacements from the center of the pillar. The pillar diameter was fixed at 100 nm, while the lateral displacement was varied from 0 to the edge of the pillar at 50 nm. In this study, the 15 nm and 85 nm deep emitters were inspected to represent the maximum and the minimum point of the depth dependency.

As observed in the result in Fig. 9, the apparent maximum efficiency from the 85 nm deep emitters (orange) did not reduce significantly from the lateral displacements. On the other hand, the 15 nm (red) improved slightly as the emitter was displaced from the center. From these find-

ings, there seem to be no large detrimental effects from the lateral displacements from the pillar centers. This is a very fortunate result as the lateral placement is a random process. Although lateral placement control can be achieved with electron-beam lithography, the uncertainty could still be up to tens of nanometers.

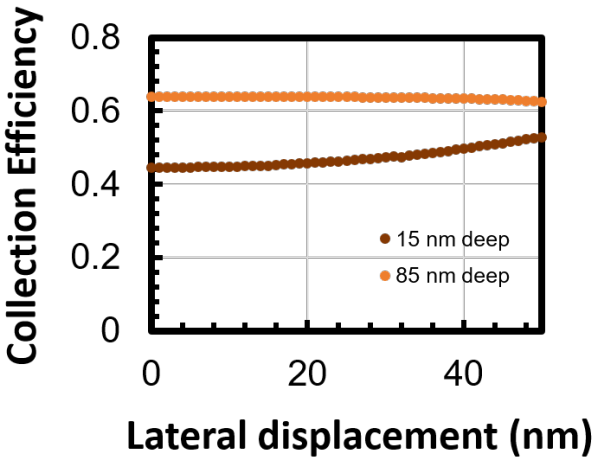

Fig. 9. A plot showing the effect of lateral misalignment from the center of the pillar. The simulation was performed for both 15 nm (red) and 85 nm (orange) deep nitrogen-vacancy center

4. Conclusion

This work has presented a simulation framework based on the FEM for studying the emission pattern and the signal's collection efficiency from the nitrogen-vacancy center emitter in diamond. The main goal here is to study a photonic structure based on nanopillar for improving the collection efficiency from the quantum emitter. From the introduced framework, various pillar diameters were examined to find the optimum dimension for the zero-phonon-line emission. The emission wavelength spectrum dependency was also inspected, where the optimum pillar diameter was mapped out throughout the spectrum. For real-world applications, the emitter placement inside the diamond pillar can have some amount of uncertainty. Hence, this work also further explored the effect of the emitter's depth placement and the lateral displacement inside the nanopillar.

Overall, the collection efficiency value is rather convoluted by all the factors including the pillar dimensions, the emission wavelengths, and the emitter's depth. On the other hand, the emitter's lateral displacement did not have a large effect on the efficiency. The maximum simulated efficiency was approximately 60 percent for [111] oriented defects, which is nearly 3 times the collection efficiency from the bulk emitters. This optimum efficiency can be obtained in pillar diameters ranging from 70-100 nm, with their corresponding wavelength and emitter depth.

While more experimental work is still being developed, this work provides a new understanding on how each variable is affecting the collection efficiency. Additionally, the data here can help initiate a robust design, which can work with a wider spectrum and higher tolerance displacement uncertainty. The experimental data can also provide feedback toward developing a more accurate modeling platform for other structures. With the presented possibility of improving signal collection, one can hope to develop quantum technology toward real-world usage without the need of sophisticate measurement tools.

Acknowledgement

This work was supported by the Thailand Research Fund (TRF) and Office of the Higher Education Commission (OHEC) MRG6280188.

References

[1] B. Lojek, *History of Semiconductor Engineering*. Springer Berlin Heidelberg, Jul. 2007.

[2] H. Iwai and S. N. Ohmi, "Silicon integrated circuit technology from past to future," *Microelectronics Reliability*, vol. 42, no. 4-5, pp. 465–491, Apr. 2002.

[3] R. R. Schaller, "Moore's law: Past, present, and future," *IEEE Spectrum*, vol. 34, no. 6, pp. 52–55, 57, Jun. 1997.

[4] F. L. Yang, D. H. Lee, H. Y. Chen, C. Y. Chang, S. D. Liu, C. C. Huang, T. X. Chung, H. W. Chen, C. C. Huang, Y. H. Liu, C. C. Wu, C. C. Chen, S. C. Chen, Y. T. Chen, Y. H. Chen, C. J. Chen, B. W. Chan, P. F. Hsu, J. H. Shieh, H. J. Tao, Y. C. Yeo, Y. Li, J. W. Lee, P. Chen, M. S. Liang, and C. Hu, "5nm-gate nanowire FinFET," in *Digest of Technical Papers - Symposium on VLSI Technology*, 2004, pp. 196–197.

[5] P. W. Shor, "Polynomial-time algorithms for prime factorization and discrete logarithms on a quantum computer," *Siam Review*, vol. 41, no. 2, pp. 303–332, 2006. [Online]. Available: http://dx.doi.org/10.1137/S0097539795293172

[6] B. Trauzettel, D. V. Bulaev, D. Loss, and G. Burkard, "Spin qubits in graphene quantum dots," *Nature Physics*, vol. 3, no. 3, pp. 192–196, Mar. 2007. [Online]. Available: https://www.nature.com/articles/nphys544

[7] J. Clarke and F. K. Wilhelm, "Superconducting quantum bits," *Nature*, vol. 453, no. 7198, pp. 1031–1042, 2008. [Online]. Available: http://dx.doi.org/10.1038/nature07128

[8] J. McKeever, A. Boca, A. D. Boozer, R. Miller, J. R. Buck, A. Kuzmich, and H. J. Kimble, "Deterministic

generation of single photons from one atom trapped in a cavity." *Science (New York, N.Y.)*, vol. 303, no. 5666, pp. 1992–4, Mar. 2004. [Online]. Available: http://www.ncbi.nlm.nih.gov/pubmed/14988512

[9] T. Harty, D. Allcock, C. Ballance, L. Guidoni, H. Janacek, N. Linke, D. Stacey, and D. Lucas, "High-fidelity preparation, gates, memory, and readout of a trapped-ion quantum bit," *Physical Review Letters*, vol. 113, no. 22, p. 220501, Nov. 2014. [Online]. Available: http://link.aps.org/doi/10.1103/PhysRevLett.113.220501

[10] J. R. Weber, W. F. Koehl, J. B. Varley, A. Janotti, B. B. Buckley, C. G. Van de Walle, and D. D. Awschalom, "Quantum computing with defects," *Proceedings of the National Academy of Sciences*, vol. 107, no. 19, pp. 8513–8518, May 2010. [Online]. Available: http://www.pnas.org/cgi/doi/10.1073/pnas.1003052107

[11] D. P. DiVincenzo, "The physical implementation of quantum computation," *Fortschritte der Physik: Progress of Physics*, vol. 48, no. 9–11, pp. 771–783, 2000. [Online]. Available: https://onlinelibrary.wiley.com/doi/10.1002/

[12] G. Balasubramanian, P. Neumann, D. Twitchen, M. Markham, R. Kolesov, N. Mizuochi, J. Isoya, J. Achard, J. Beck, J. Tissler, V. Jacques, P. R. Hemmer, F. Jelezko, and J. Wrachtrup, "Ultralong spin coherence time in isotopically engineered diamond," *Nature Materials*, vol. 8, no. 5, pp. 383–387, May 2009. [Online]. Available: http://www.nature.com/doifinder/10.1038/nmat2420

[13] N. Bar-Gill, L. Pham, A. Jarmola, D. Budker, and R. Walsworth, "Solid-state electronic spin coherence time approaching one second," *Nature Communications*, vol. 4, p. 1743, Apr. 2013. [Online]. Available: http://www.nature.com/doifinder/10.1038/ncomms2771

[14] B. J. Maertz, A. P. Wijnheijmer, G. D. Fuchs, M. E. Nowakowski, and D. D. Awschalom, "Vector magnetic field microscopy using nitrogen vacancy centers in diamond," *Applied Physics Letters*, vol. 96, no. 9, p. 92504, Mar. 2010. [Online]. Available: https://doi.org/10.1063/1.3337096

[15] H. Bernien, L. Childress, L. Robledo, M. Markham, D. Twitchen, and R. Hanson, "Two-photon quantum interference from separate nitrogen vacancy Centers in diamond," *Phys. Rev. Lett.*, vol. 108, no. 4, Jan. 2012. [Online]. Available: http://dx.doi.org/10.1103/physrevlett.108.043604

[16] H. Bernien, B. Hensen, W. Pfaff, G. Koolstra, M. S. Blok, L. Robledo, T. H. Taminiau, M. Markham, D. J. Twitchen, L. Childress, and R. Hanson, "Heralded entanglement between solid-state qubits separated by three metres," *Nature*, vol. 497, no. 7447, pp. 86–90, Apr. 2013. [Online]. Available: http://www.nature.com/doifinder/10.1038/nature12016http://www.nature.com/nature/journal/v497/n7447/full/nature12016.html%5Cnhttp://www.nature.com/nature/journal/v497/n7447/pdf/nature12016.pdf

[17] B. Hensen, H. Bernien, A. E. Dréau, A. Reiserer, N. Kalb, M. S. Blok, J. Ruitenberg, R. F. L. Vermeulen, R. N. Schouten, C. Abellán, W. Amaya, V. Pruneri, M. W. Mitchell, M. Markham, D. J. Twitchen, D. Elkouss, S. Wehner, T. H. Taminiau, and R. Hanson, "Loophole-free Bell inequality violation using electron spins separated by 1.3 kilometres," *Nature*, vol. 526, no. 7575, pp. 682–686, Oct. 2015. [Online]. Available: http://www.nature.com/doifinder/10.1038/nature15759

[18] W. Pfaff, B. J. Hensen, and H. Bernien et al., "Quantum information. Unconditional quantum teleportation between distant solid-state quantum bits." *Science (New York, N.Y.)*, vol. 345, no. 6196, pp. 532–5, Aug. 2014. [Online]. Available: http://www.ncbi.nlm.nih.gov/pubmed/25082696

[19] G. D. Fuchs, G. Burkard, P. V. Klimov, and D. D. Awschalom, "A quantum memory intrinsic to single nitrogen–vacancy centres in diamond," *Nature Physics*, vol. 7, no. 10, pp. 789–793, Jun. 2011. [Online]. Available: http://www.nature.com/doifinder/10.1038/nphys2026

[20] J. M. Taylor, P. Cappellaro, L. Childress, L. Jiang, D. Budker, P. R. Hemmer, A. Yacoby, R. Walsworth, and M. D. Lukin, "High-sensitivity diamond magnetometer with nanoscale resolution," *Nat Phys*, vol. 7, no. 3, p. 270, 2011. [Online]. Available: http://dx.doi.org/10.1038/nphys1937

[21] F. Dolde, "Electric-field sensing using single diamond spins," *Nat. Phys.*, vol. 7, pp. 459–463, 2011. [Online]. Available: http://dx.doi.org/10.1038/nphys1969

[22] D. A. Hopper, H. J. Shulevitz, and L. C. Bassett, "Spin Readout Techniques of the Nitrogen-Vacancy Center in Diamond," *Micromachines 2018, Vol. 9, Page 437*, vol. 9, no. 9, p. 437, Aug. 2018. [Online]. Available: https://www.mdpi.com/2072-666X/9/9/437/htmhttps://www.mdpi.com/2072-666X/9/9/437

[23] M. Jamali, I. Gerhardt, M. Rezai, K. Frenner, H. Fedder, and J. Wrachtrup, "Microscopic diamond solid-immersion-lenses fabricated around single defect centers by focused ion beam milling," *Review of Scientific Instruments*, vol. 85, no. 12, p. 123703, Dec. 2014. [Online]. Available: https://aip.scitation.org/doi/abs/10.1063/1.4902818

[24] M. J. Burek, N. P. de Leon, B. J. Shields, B. J. M. Hausmann, Y. Chu, Q. Quan, A. S. Zibrov, H. Park, M. D. Lukin, and M. Lončar, "Free-standing mechanical and photonic nanostructures in single-crystal diamond," *Nano Letters*, vol. 12, no. 12, pp. 6084–6089, Dec. 2012. [Online]. Available: http://pubs.acs.org/doi/abs/10.1021/nl302541e

[25] J. Tisler, G. Balasubramanian, B. Naydenov, R. Kolesov, B. Grotz, R. Reuter, J.-P. Boudou, P. A. Curmi, M. Sennour, A. Thorel, M. Börsch, K. Aulenbacher, R. Erdmann, P. R. Hemmer, F. Jelezko, and J. Wrachtrup, "Fluorescence and spin properties of defects in single digit nanodiamonds," *ACS Nano*, vol. 3, no. 7, pp. 1959–1965, Jul. 2009. [Online]. Available: http://pubs.acs.org/doi/abs/10.1021/nn9003617

[26] B. J. Hausmann, M. Khan, Y. Zhang, T. M. Babinec, K. Martinick, M. McCutcheon, P. R. Hemmer, and M. Lončar, "Fabrication of diamond nanowires for quantum information processing applications," *Diamond and Related Materials*, vol. 19, no. 5-6, pp. 621–629, May 2010. [Online]. Available: http://linkinghub.elsevier.com/retrieve/pii/S0925963510000312

[27] B. J. M. Hausmann, B. Shields, Q. Quan, P. Maletinsky, M. McCutcheon, J. T. Choy, T. M. Babinec, A. Kubanek, A. Yacoby, M. D. Lukin, and M. Loncar, "Integrated diamond networks for quantum nanophotonics." *Nano letters*, vol. 12, no. 3, pp. 1578–82, Mar. 2012. [Online]. Available: http://www.ncbi.nlm.nih.gov/pubmed/22339606

[28] Y.-C. Liu, K. Chang, J. Fwu, and L. Shih, "Performance comparison between fdtd and fem for the simulation of plasmonic waveguide operating at optical communication frequency," in *2013 USNC-URSI Radio Science Meeting (Joint with AP-S Symposium)*. Institute of Electrical and Electronics Engineers (IEEE), Jan. 2014, pp. 184–184.

[29] P. Ovartchaiyapong, "Simulation of optimal photonic nanopillar design for solid-state quantum emitter in diamond," in *17th International Conference on Electrical Engineering/Electronics, Computer, Telecommunications and Information Technology, ECTI-CON 2020*. Institute of Electrical and Electronics Engineers Inc., Jun. 2020, pp. 599–602.

[30] E. Neu, P. Appel, M. Ganzhorn, J. Miguel-Sánchez, M. Lesik, V. Mille, V. Jacques, A. Tallaire, J. Achard, and P. Maletinsky, "Photonic nano-structures on (111)-oriented diamond," *Applied Physics Letters*, vol. 104, no. 15, p. 153108, Apr. 2014. [Online]. Available: https://aip.scitation.org/doi/abs/10.1063/1.4871580

Preeti Ovartchaiyapong was born in Bangkok, Thailand. He received his Ph.D. from University of California Santa Barbara in 2016. Since 2017, he has been a faculty member at the Department of Electrical and Computer Engineering, Thammasat University. His research interests include solid-state quantum systems, nanofabrications, photonics, optics and lasers.